The stability of quasi 2D lattices of magnetic holes

1985 J. Phys. A: Math. Gen. 18 2325

(http://iopscience.iop.org/0305-4470/18/12/030)

J. Phys. A: Math. Gen. 18 (1985) 2325-2341. Printed in Great Britain

The stability of quasi 2D lattices of magnetic holes

M Warner† and R M Hornreich‡

† Rutherford Appleton Laboratory, Chilton, Didcot, Oxon OX11 0QX, UK
‡ Department of Theoretical Physics, Oxford University, OX1 3NP, UK and
§ Department of Electronics, Weizmann Institute of Science, Rehovot, Israel

Received 15 February 1985

Abstract. It has recently been demonstrated by Skjeltorp that a monolayer of non-magnetic inclusions in a paramagnetic fluid crystallises when a perpendicular magnetic field is applied. Temperature is scaled by this field and 2D melting has been observed. Here we examine the *energetics* of the stability of the regular structures formed. Competing dipolar interactions and a frustration under distortions give a range of possibilities including a strictly 2D triangular lattice, a quasi 2D distorted triangular lattice and a quasi 2D square lattice. A second melting possibility becomes evident, but we restrict our analysis of the interactions to zero temperature.

The underlying lattice energies are all close and the delicacy involved in calculating their energies, arising from the long-range character of the forces involved, requires a modification of the Ewald technique. We perform stability analysis to find instability modes and their amplitudes.

1. Introduction

Recently, Skjeltorp (1983, 1984) has shown that a monolayer of micron diameter monodispersed polystyrene spheres in a magnetic colloid (see, e.g. Rosensweig 1979) will crystallise on a triangular lattice in the presence of a magnetic field applied perpendicular to the layer. This novel result is a consequence of the effective magnetic dipole moment associated with each sphere due to the polarisation of the surrounding magnetic fluid by the field. These dipoles, actually dipole holes, repel each other leading to a crystallisation when the concentration of spheres is held constant.

As noted by Skjeltorp, this system could provide an interesting model for studying collective phenomena, as a function of temperature, in two dimensions. It therefore appears worthwhile to examine it in more detail and, in particular, to determine the energetically stable configuration as a function of the system parameters. This is the main objective of this paper. We shall show that, neglecting temperature, a strictly 2D triangular structure is, in fact, stable only when the ratio of magnetic layer thickness to inter-sphere separation is below a critical value. Above this value, a quasi 2D triangular structure is stable, while at still larger values of this ratio it appears that a quasi 2D structure characterised by a square lattice is the globally stable state.

Our approach is as follows: in § 2, we develop the theoretical framework needed to calculate the interaction energy of 2D arrays of non-magnetic spherical inclusions

§ Present and permanent address.

0305-4470/85/122325+17$02.25

immersed in a strongly paramagnetic fluid layer. Both triangular and square lattice arrays are considered. The possibility that these systems can lower their energy by a spontaneous distortion into a quasi 2D pattern is also considered. Next, in § 3, we discuss how the lattice sums for the different interaction energies can be efficiently and accurately evaluated by a combination of analytic and numerical techniques. In order to do this the classical Ewald method must be appropriately modified. This is carried out in the appendix. The lattice sum evaluations and the resulting interaction energies for the two undistorted and three distorted lattice configurations being considered are then given as functions of two parameters—one characterising the magnetic properties of the fluid and the second the relative thickness, Δ, of the magnetic layer compared with the average spacing between inclusions. The first parameter, the paramagnetic susceptibility of the fluid, determines the strength of image effects compared with dipolar interactions within the layer. The second parameter, Δ, expresses how effectively these image forces, a consequence of the layer having a surface, *compete* with the direct interactions and determine the structure. Finally in § 4, we discuss the results of our analysis and compare them with those reported by Skjeltorp. Promising lines for future investigations are indicated.

2. Theoretical analysis

2.1. General considerations

We begin our analysis with the simple case of an isolated sphere of radius ρ and permeability μ_s suspended in a magnetic fluid of permeability μ_f. SI units will be used throughout. In a uniform field $\boldsymbol{H}$, the change in the scalar potential outside the sphere is (see, e.g., Bleaney and Bleaney 1978)

$$\Delta\Phi = \left(\frac{\mu_s - \mu_f}{\mu_s + 2\mu_f}\right)\rho^3 \frac{\boldsymbol{H}\cdot\boldsymbol{r}}{r^3} \equiv \frac{\boldsymbol{\sigma}\cdot\boldsymbol{r}}{4\pi r^3} \tag{1}$$

where

$$\boldsymbol{\sigma} = 4\pi\left(\frac{\mu_s - \mu_f}{\mu_s + 2\mu_f}\right)\rho^3 \boldsymbol{H} \tag{2a}$$

is the effective dipole moment of the sphere. For $\mu_s = \mu_0$, $\mu_f = \mu_0(1+\chi_f)$, this becomes

$$\boldsymbol{\sigma} = -\frac{4\pi\rho^3}{3}\left(\frac{\chi_f}{1+\frac{2}{3}\chi_f}\right)\boldsymbol{H} = -V\bar{\chi}_f \boldsymbol{H} \tag{2b}$$

where V is the volume of the sphere and χ_f is the effective susceptibility.

We next consider a collection of physically identical spheres, having moments $\boldsymbol{\sigma}_i$ and separated by distances $\boldsymbol{r}_{ij}$. The total interaction energy of such a system is (Bleaney and Bleaney 1978)

$$\begin{aligned} U &= -\sum_{i<j} \boldsymbol{\sigma}_i \cdot \boldsymbol{B}_j(\boldsymbol{r}_i) \\ &= \frac{\mu_f}{4\pi}\sum_{i<j}\left[\left(\boldsymbol{\sigma}_i\cdot\boldsymbol{\sigma}_j - \frac{3(\boldsymbol{\sigma}_i\cdot\boldsymbol{r}_{ij})(\boldsymbol{\sigma}_j\cdot\boldsymbol{r}_{ij})}{r_{ij}^2}\right)\Big/ r_{ij}^3\right]. \end{aligned} \tag{3a}$$

When the moments $\boldsymbol{\sigma}_i$ are all aligned, (3*a*) takes the simpler form

$$U = \frac{\mu_f}{4\pi} \sum_{i<j} \sigma_i \sigma_j \left(\frac{1 - 3\cos^2 \theta_{ij}}{r_{ij}^3} \right) \tag{3b}$$

where θ_{ij} is the angle between $\boldsymbol{\sigma}_i$ and $\boldsymbol{r}_{ij}$. However, (2) can be substituted directly into (3) only when $\boldsymbol{\sigma}_i$ is independent of the dipolar field of the site *i*. This, of course, is not the case here. When the dipolar field at site *i* is aligned with $\boldsymbol{H}$, a dipole σ', corrected to first order and valid when $\rho \ll (r_{ij})_{\min}$, can be obtained by replacing $\boldsymbol{\sigma}_i$ by

$$\sigma_i' = -V\bar{\chi}_f H \Big/ \left[1 + \frac{1}{8\pi} V\bar{\chi}_f \sum_{j \neq i} \alpha_{ij} \left(\frac{1 - 3\cos^2 \theta_{ij}}{r_{ij}^3} \right) \right]. \tag{4}$$

Here $\alpha_{ji} = \sigma_j'/\sigma_i'$ is a geometrical factor independent of $\boldsymbol{H}$.

Up to this point the magnetic field in which the polystyrene spheres are suspended has been regarded as occupying all of space. In fact, it is restricted to a finite 2D layer of thickness *h* as illustrated in figure 1. This has two consequences. One, the applied field $\boldsymbol{H}$ within the magnetic fluid is related to the externally applied field $\boldsymbol{H}_a$ by

$$\boldsymbol{H} = \boldsymbol{H}_a/\mu_f. \tag{5}$$

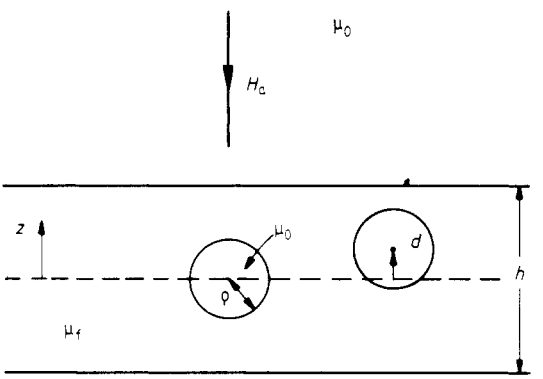

Figure 1. Schematic of spherical inclusions in a magnetic layer. The applied field $\boldsymbol{H}_a$ is perpendicular to the layer width *h*, of ferro-fluid of permittivity μ_f. Perpendicular displacement *d* is measured from the (broken) centre of the fluid. Spherical inclusions, of radius ρ, are shown at the points $z = 0$ and $z = d$. They have the same permittivity, μ_0, as the medium exterior to the fluid.

Two, the dipolar field must satisfy the usual boundary conditions at the top and bottom surfaces of the magnetic layer. A convenient way of accomplishing this is by using the method of images. Consider a single sphere displaced at a height $z = d$ from the layer centre as shown in figure 1. By analogy with the treatment of Weber (1950) for the case of dielectric media, it is straightforward to show that the dipolar field within the layer is that of the real dipole plus that of two sets of image dipoles, one located in the space $z \geqslant \frac{1}{2}h$ and the other in $z \leqslant -\frac{1}{2}h$. All the image dipoles, of course, lie on the line perpendicular to the fluid layer and passing through the centre of the sphere. Their positions and magnitudes are given by

$$z_l = lh + (-1)^l d, \tag{6a}$$

$$\sigma_l = [-(\mu_f - \mu_0)/(\mu_f + \mu_0)]^{|l|}\sigma$$
$$\equiv (-\eta)^{|l|}\sigma, \qquad l = \pm 1, \pm 2, \ldots . \tag{6b}$$

Images in the upper half space have $l > 0$ and in the lower $l < 0$. All the dipoles, both real and image, are regarded as lying in a medium with permeability μ_f.

When a collection of real dipoles σ_i, located at positions (x_i, y_i, d_i), are in the magnetic layer (6) is simply generalised to

$$z_{il} = lh + (-1)^l d_i, \tag{7a}$$

$$\sigma_{il} = (-\eta)^{|l|}\sigma_i, \qquad l = \pm 1, \pm 2, \ldots, i = 1, 2, \ldots . \tag{7b}$$

To take account of the additional polarisation due to the dipolar field we again use (4), with the sum on j now being over all other real dipoles and all image dipoles. Note that, for a given real dipole, all its image dipoles satisfy

$$\alpha_{li} = \sigma'_{il}/\sigma'_i = \sigma_{il}/\sigma_i = (-\eta)^{|l|}. \tag{8}$$

The total interaction energy of the system is now obtained by including in U the energies of attraction between pairs of real and image dipoles. Note that these energies are, however, equal to *one-half* the energies of interaction between equivalent real dipoles. Thus (3*b*) is replaced by

$$U = \frac{\mu_f}{8\pi} \sum_{i \neq j} \sigma'_i \sigma'_j \left(\frac{1 - \cos^2 \theta_{ij}}{r_{ij}^3} \right), \tag{9}$$

with the i sum being taken over real dipoles only and the j sum over both real and image dipoles. (When i and j refer to a pair of real dipoles, the additional factor of $\frac{1}{2}$ in (9) over and above (3*b*) is to avoid double counting).

2.2. The two-dimensional triangular and square lattices

When thermal fluctuations are negligible, the vertical position of an isolated polystyrene sphere is determined by the buoyancy and magnetic forces acting upon it. In a sufficiently strong applied field, the latter is the dominant effect and results in the sphere positioning itself in the middle of the layer. This is related to the magnetic levitation effect first reported by Rosensweig (1966). Assuming for the moment that this centring also holds for *each* of N individual spheres when they are packed in a monolayer at a density of D spheres/cm^2, we now determine whether a triangular or square lattice configuration has the lower energy. Although these configurations are obviously two dimensional, their self-energies are, in a sense, intermediate between those of 2D ferro- and 3D antiferromagnetic systems. That is, as μ_f increases from unity to infinity we interpolate smoothly between these two limiting cases. We shall return to this point in § 3.

Consider first the triangular (T) lattice. The lattice spacing a, given by

$$a = (2/\sqrt{3})^{1/2}/D^{1/2} \tag{10}$$

is a convenient length scale and we therefore define a normalised layer thickness $\Delta = h/a$. By symmetry, the moment ratios α_{ij} are simply given by $\alpha_{ij} = (-\eta)^{|l|}$, with $l = 0$ corresponding to the case wherein index j denotes a real dipole. Defining

$$u = U/(V^2 \bar{\chi}_f^2 H_a^2 \mu_f / 8\pi a^3) \tag{11}$$

we have

$$(u_0)_T = \sum_T \Big/ \left(1 + \gamma \sum_T\right)^2, \tag{12a}$$

with

$$\gamma = (1/8\pi) V\bar{\chi}_f / a^3 \tag{12b}$$

and

$$\sum_T = \sum_{n,m,l} (-\eta)^{|l|}(1 - 3l^2\Delta^2/f_T)/f_T^{3/2}, \tag{12c}$$

$$f_T(\Delta) = (n^2 + m^2 + nm + l^2\Delta^2). \tag{12d}$$

The sum in (12*c*) is over all integer values of n, m and l except for $n = m = l = 0$.

We now turn to the square (S) lattice. Here the lattice spacing b is

$$b = D^{-1/2} = (\sqrt{3}/2)^{1/2} a, \tag{13}$$

and we have

$$(u_0)_S = (2/\sqrt{3})^{3/2} \sum_S \Big/ \left(1 + (2/\sqrt{3})^{3/2} \gamma \sum_S\right)^2, \tag{14a}$$

$$\sum_S = \sum_{n,m,l} (-\eta)^{|l|}(1 - 3l^2\Delta_S^2/f_S)/f_S^{3/2}, \tag{14b}$$

$$f_S(\Delta_S) = (n^2 + m^2 + l^2\Delta_S^2), \tag{14c}$$

$$\Delta_S^2 = 2\Delta^2/\sqrt{3}. \tag{14d}$$

As before, the point $n = m = l = 0$ is excluded from the sum in (14*b*). The evaluation of the lattice sums Σ_T, Σ_S will be discussed in § 3.

2.3. The distorted triangular and square lattices

In § 2.2 it was assumed that the magnetic forces order all the polystyrene spheres in a single monolayer. We shall now show that this assumption is valid only when Δ, the normalised layer thickness, is sufficiently small. To demonstrate this let us consider a perturbation of the monolayer state wherein each of the spheres is moved vertically a distance $d_i \ll h$. Whenever such a perturbation results in an increase in the system energy, the monolayer lattice is stable. If, however, there exists *any* set $\{d_i\}$ for which the energy is *decreased*, the unperturbed 2D lattice is no longer stable.

In principle, therefore, we should calculate the system energy for an arbitrary set of displacements $\{d_i\}$. While this is possible, we chose to employ a simpler procedure in which specific distortion modes, selected by physical considerations, were analysed. This, of course, gives only upper bounds on the true ground-state energy. However, this procedure does, we believe, illustrate clearly the behaviour of the system.

We begin by noting that the reason a distortion mode appears is that when only the interaction between a pair of real dipoles with $\boldsymbol{r}_{12} \perp \boldsymbol{\sigma}_1$, $\boldsymbol{\sigma}_2$ and $\boldsymbol{\sigma}_1 \| \boldsymbol{\sigma}_2$ is considered, the system energy is *always* lowered when one of the dipoles is raised and the other lowered parallel to the moment axis. Thus if the colloid layer is sufficiently thick relative to the dipole spacing, a distortion of the 2D monolayer is always energetically preferred. For a very thin colloid layer on the other hand, each dipole interacts more

strongly with its own images than with the neighbouring real dipoles. The total interaction energy is then minimised by the dipoles remaining in the middle of the colloid layer.

Since dipole-dipole interactions fall off rapidly with distance, it is clear that physically optimal distortion modes will generally be those in which neighbouring dipoles are displaced in opposite directions. Consider first the square lattice. Here a simple mode satisfying the above criterion is obtained by dividing the system into two sublattices such that the nearest neighbours of a given dipole are all on the other sublattice. This is illustrated in figure 2(*a*). We distort the monolayer configuration by raising all the dipoles belonging to one sublattice by d and simultaneously lowering all those on the other sublattice by the same distance.

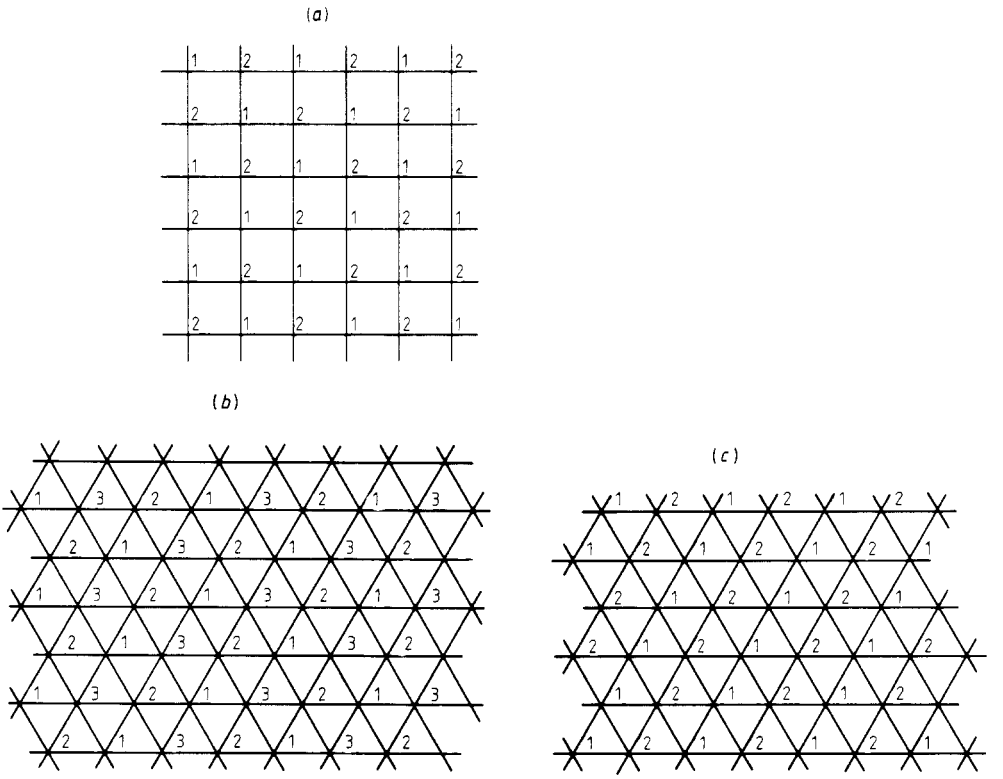

Figure 2. Displacement modes for the real dipole positions analysed in the text for their stability with respect to the undistorted 2D array. Numbers at lattice points indicate (1) ≡ up, (2) ≡ down, and (3) ≡ unshifted. The figures are (*a*) distorted square lattice, denoted by S, (*b*) three-sublattice distortion of a triangular array, denoted by T_Δ and (*c*) two-sublattice distortion of a triangular array, denoted by $T_\parallel$.

For the triangular lattice, however, such a simple division into two sublattices is no longer possible. Considering the dominance of nearest neighbours, the situation is closely analogous to that of the triangular antiferromagnet, namely, one of total frustration. In each triangular plaquette, moving one dipole up and another down in order to minimise their interaction energy leaves the third dipole frustrated. We therefore consider two alternate distortion modes which are physically appealing.

In the first, shown in figure 2(b), we divide the system into *three* sublattices, such that all the nearest neighbours of a given dipole lie on the other two sublattices. We then distort the monolayer configuration by raising one sublattice by d, lowering the second by this amount, and leaving the third undisturbed in the middle of the third layer. Note that this mode preserves the three-fold rotation symmetry of the undistorted lattice. As indicated above, when allowing only the possibility for up or down in analogy to the square lattice distortions, the frustration is total and can be identified with the spin-$\frac{1}{2}$ Ising triangular antiferromagnet. Allowing the third alternative of no motion gives a similarity to the spin-1 Ising system discussed by Blume *et al* (1971). Our case corresponds to that of an antiferromagnet with an easy plane when the amplitude of distortion is small. This is because the energy of interaction between a raised (or lowered) dipole and a lower (or raised) dipole is four times that of the interaction with a stationary one, see (16). Assembling these energies and denoting two neighbouring spins as S_1 and S_2 one obtains for the Hamiltonian $\mathcal{H}$:

$$\mathcal{H} \propto -(S_1^2 + S_2^2 - 2S_1S_2) \equiv -(S_1 - S_2)^2.$$

For larger amplitudes this term is amended and an additional $(S_1S_2)^2$ term is required. One should remember however this is merely an illustration of the local frustration and that the real problem has long range forces, decaying like $1/r^5$ considering distortional energy changes.

In the second distortion mode, shown in figure 2(c), we divide the triangular lattice into only *two* sublattices. In this case, only four of the six nearest neighbours of a given dipole are on the other sublattice and the three-fold symmetry of the original lattice is lost. In the distorted state, dipoles on one of the sublattices are raised by d and on the other are lowered through the same distance. Note that this configuration is similar in some respects to the distorted square lattice.

Defining the normalised displacement

$$\xi = d/a \tag{15}$$

we wish to determine $\xi = \xi(\Delta, \eta)$ and the interaction energies for the three specific distortion modes shown in figure 2. In the vicinity of the spontaneous distortion threshold, $\xi^2 \ll 1$ and we can conveniently expand the relevant interaction energies in ξ. Neglecting the dipole moment correction (this will be justified in § 4), we obtain expressions of the form

$$u = u_0 + u_2\xi^2 + u_4\xi^4 + \ldots \tag{16}$$

with $u_4 > 0$ for all three distortion modes. The spontaneous distortion thresholds are thus determined by setting $u_2(\Delta, \eta) = 0$. When $u_2 > 0$, $\xi = 0$, $u = u_0$ and when $u_2 < 0$,

$$\xi^2 = \bar{\xi}^2 = -u_2/2u_4, \qquad u = u_0 - u_2^2/4u_4. \tag{17a, b}$$

For the square lattice distortion mode of figure 2(a), we have

$$(u_2)_S = -\left(\frac{2}{\sqrt{3}}\right)^{5/2}\frac{3}{4}\left(\sum_{(a1)}\frac{(-\eta)^{|l|}S_2(\Delta_S)}{f_S^{5/2}(\Delta_S)} + \frac{1}{4\sqrt{2}}\sum_{(a2)}\frac{(-\eta)^{|l|}S_2(\Delta_S/\sqrt{2})}{f_S^{5/2}(\Delta_S/\sqrt{2})}\right) \tag{18a}$$

$$S_2(\Delta_S) = (3 - 30l^2\Delta_S^2/f_S + 35l^4\Delta_S^4/f_S^2) \tag{18b}$$

$$(u_4)_S = \left(\frac{2}{\sqrt{3}}\right)^{7/2}\frac{75}{16}\left(\sum_{(a1)}\frac{(-\eta)^{|l|}S_4(\Delta_S)}{f_S^{7/2}(\Delta_S)} + \frac{1}{8\sqrt{2}}\sum_{(a2)}\frac{(-\eta)^{|l|}S_4(\Delta_S/\sqrt{2})}{f_S^{7/2}(\Delta_S/\sqrt{2})}\right) \tag{18c}$$

$$S_4(\Delta_S) = (1 - 21l^2\Delta_S^2/f_S + 63l^4\Delta_S^4/f_S^2 - 46\times 2l^6\Delta_S^6/f_S^3). \tag{18d}$$

The sum $(a1)$ is over all integers (n, m, l) satisfying $(n-m) = 1 \bmod 2$, with l even while the sum $(a2)$ is over all (n, m, l) with l odd.

For the triangular lattice distortion mode T_Δ shown in figure 2(b), the relevant expressions are

$$(u_2)_{T_\Delta} = -\left(9\sum_{(b1)}\frac{(-\eta)^{|l|}t_2(\Delta)}{f_T^{5/2}(\Delta)} + 3\sum_{(b2)}\frac{(-\eta)^{|l|}t_2(\Delta)}{f_T^{5/2}(\Delta)} + \frac{2}{3^{5/2}}\sum_{(b3)}(-\eta)^{|l|}t_2(\Delta/\sqrt{3})/f_T^{5/2}(\Delta/\sqrt{3})\right), \tag{19a}$$

$$t_2(\Delta) = (3 - 30l^2\Delta^2/f_T + 35l^4\Delta^4/f_T^2), \tag{19b}$$

$$(u_4)_{T_\Delta} = 225\left(\frac{3}{4}\sum_{(b1)}\frac{(-\eta)^{|l|}t_4(\Delta)}{f_T^{7/2}(\Delta)} + \frac{1}{12}\sum_{(b2)}\frac{(-\eta)^{|l|}t_4(\Delta)}{f_T^{7/2}(\Delta)} + \frac{2}{3^{11/2}}\sum_{(b3)}(-\eta)^{|l|}t_4(\Delta/\sqrt{3})/f_T^{7/2}(\Delta/\sqrt{3})\right) \tag{19c}$$

$$t_4(\Delta) = (1 - 21l^2\Delta^2/f_T + 63l^4\Delta^4/f_T^2 - 46\times 2l^6\Delta^6/f_T^3). \tag{19d}$$

The sums $(b1)$ and $(b2)$ are over integers (n, m, l) satisfying $n = 0 \bmod 3$ and $m = 1 \bmod 3$, with l even and l odd, respectively. The sum $(b3)$ is over all (n, m, l) with l odd.

Finally, for the triangular lattice distortion mode $T_\parallel$ illustrated in figure 2(c), we obtain

$$(u_2)_{T_\parallel} = -\frac{3}{4}\left(\sum_{(c1)}\frac{(-\eta)^{|l|}t_2(\Delta)}{f_T^{5/2}(\Delta)} + \sum_{(c2)}\frac{(-\eta)^{|l|}t_2(\Delta)}{f_T^{5/2}(\Delta)}\right) \tag{20a}$$

$$(u_4)_{T_\parallel} = \frac{75}{16}\left(\sum_{(c1)}\frac{(-\eta)^{|l|}t_4(\Delta)}{f_T^{7/2}(\Delta)} + \sum_{(c2)}\frac{(-\eta)^{|l|}t_4(\Delta)}{f_T^{7/2}(\Delta)}\right) \tag{20b}$$

with the sums $(c1)$, $(c2)$ over all integers (n, m, l) satisfying n odd, l even and n even, l odd, respectively.

3. Results for the lattice energy calculations

3.1. Calculation of the undistorted lattice energies

We first outline the method used to calculate the interaction energy of a 3D system formed by a planar array of dipoles and its infinite set of images. This system of dipoles has analogues in the classical theory of elementary magnetic dipoles. When the relative image strength $(-\eta)^{|l|}$ (where l denotes the number of the image plane) vanishes ($\eta \to 0$), the fluid slab is of the same composition as the outside and we have a simple, ferromagnetically ordered planar lattice. When the ferro-fluid permittivity, μ_f, becomes much larger than that (μ_0) external to the fluid, the image strengths become equal to those of the real dipoles ($\eta \to 1$). Since the image dipole orientations alternate from plane to plane, the array of identical dipoles is ferromagnetically ordered within planes and antiferromagnetically ordered between planes. These two well known limits (Cohen and Keffer 1955) will allow us to check the accuracy of our numerical results.

We are interested in the interaction energy per real dipole as a result of its interactions with the other real dipoles (in the same plane) and with all the images. Since the image strengths vary from plane to plane it is best not to calculate the energy directly as a 3D sum, but instead as the sum of the interactions of the real dipole with the fields resultant at its site from each plane. Each such field, resulting from a given plane, is then accorded the appropriate weight, $(-\eta)^{|l|}$, in the sum over all planes.

Before calculating the field at the origin resulting from the dipoles in an arbitrary plane we give a simple argument for the variation with distance to the plane of the field strength emanating from that plane. Let the plane under consideration be at $z=0$ and the point of observation at $\boldsymbol{R}=(0,0,z=R)$. The field from a dipole decays as $1/r^3$, so at distance r away we might also expect the total field from a plane of dipoles to be slowly decaying. The subtle convergence and boundary condition effects associated with dipolar fields in ferromagnets result from this. However, at fixed z, the potential Φ will be periodic in x and y due to the translational invariance of the dipole array at $z=0$. Further, $\nabla^2\Phi=0$ and it follows that $k_x^2+k_y^2+k_z^2=0$, the k_i's being the appropriate Fourier wavevectors characterising the spatial variation of Φ. Since the vectors k_x, k_y are real, $k_z^2\leqslant 0$ and there is an exponential decay of the potential (and field) as the distance R from the plane increases. Thus, when resolved into contributions from dipole planes, the convergence of the total field at a site will be very good. However, problems in evaluating the field due to a given plane remain since the convergence of sums involving $1/r^3$ interactions is conditional in three dimensions. Physical manifestations of this are the dependence of ferromagnetic energies on sample shape (the boundaries are always relevant) and the distinction between the transverse and longitudinal limits for a ferromagnet. This has been discussed in detail by Cohen and Keffer (1955). The slow convergence in the plane presents a practical difficulty as well. The two undistorted lattice types between which we wish to distinguish, square and triangular, have interaction energies differing typically by less than 1%. To evaluate lattice sums with an accuracy much better than this makes a direct summation out of the question and one must resort to the Ewald technique (see Nijboer and de Wette 1957). However, for a system whose properties (dipole strength) vary plane by plane as one moves away from the origin, the technique must be generalised. This is done in the appendix, where we review and extend the Ewald technique to cover our present needs. We indeed find the exponential decay expected from the general considerations given above.

The dimensionless sums to be evaluated are given in (12*c*) and (14*b*). These sums are functions of a single parameter Δ, the ratio of thickness of ferro-fluid to (triangular) lattice spacing. The latter is related to the areal number density D by (10). The interaction energy of a plane a distance R away from the site of interest is, from the appendix:

$$\Sigma_\rho(R)=\sum_{\boldsymbol{\lambda}}^{(2D)}\Bigg[\Gamma(\tfrac{5}{2},\pi(\boldsymbol{r}_{\boldsymbol{\lambda}}+\boldsymbol{R})^2)P_2(\cos\theta_{\boldsymbol{r}_{\boldsymbol{\lambda}}+\boldsymbol{R}})/|\boldsymbol{r}_{\boldsymbol{\lambda}}+\boldsymbol{R}|^3 - \frac{\pi^{3/2}}{v}\exp(-\pi R^2-\pi k_{\boldsymbol{\lambda}}^2)\Big(1-(3\pi k_{\boldsymbol{\lambda}}/4) \times\sum_{\pm}\exp[\pi(k_{\boldsymbol{\lambda}}\pm R)^2]\operatorname{erfc}(\pi^{1/2}(k_{\boldsymbol{\lambda}}\pm R))\Big)\Bigg]/\Gamma(\tfrac{5}{2}) \tag{21}$$

where $\Gamma(x)$ and $\Gamma(n,x)$ are the complete and incomplete gamma functions respectively,

$\boldsymbol{\lambda}$ labels a site in the real or reciprocal (k) space lattice, v is a cell area in the real lattice (reduced by either a^2 or b^2, as appropriate; that is, $\frac{1}{2}\sqrt{3}$ or 1 for triangular or square), P_2 is the second Legendre polynomial whose argument is the cosine of the angle θ that the dipole position vector $\boldsymbol{r}_\lambda + \boldsymbol{R}$ makes with the field direction, and erfc is the complementary error function. When $R = 0$ the sum is within the plane of real dipoles and the point $\boldsymbol{r}_\lambda = \boldsymbol{0}$ must be excluded. Details are given in the appendix.

3.2. Results for the undistorted lattice energies

The lattice sums Σ_T, Σ_S were evaluated as functions of η and Δ. As we shall discuss in § 4, in cases of experimental interest, $\bar{\chi}_f < 1$ and $\rho/a < \frac{1}{3}$. Thus $\gamma < 5 \times 10^{-3}$ and $\gamma \Sigma_T$ and $(2/\sqrt{3})^{3/2} \gamma \Sigma_S$ are both less than 0.05 for relevant values of Δ. We therefore neglect the dipole field correction terms in (12a) and (14a) and show, in figures 3 and 4, the quantities

$$u_T = \sum_T, \qquad u_S = (2/\sqrt{3})^{3/2} \sum_S. \tag{22}$$

In figure 3 the undistorted interaction energies u_T and u_S are plotted against the relative image strength η for $\Delta = 0.8$, 1.0, 1.2, and ∞. For the square lattice the values of Δ indicated correspond to the values the lattice would have if it were reformed into a triangular lattice having the *same* areal number density D. This corresponds to the scaling in (14) where, because of (13), the square lattice energy is scaled by $(2/\sqrt{3})^{3/2}$

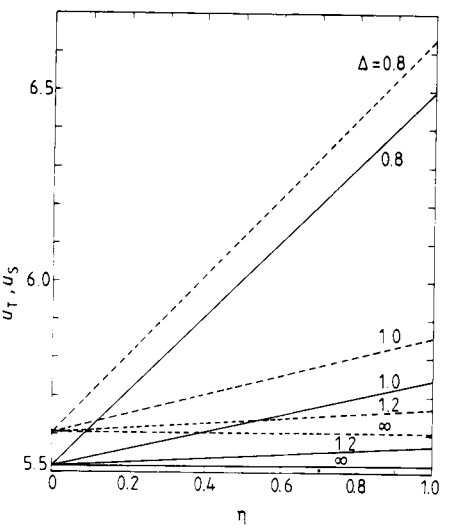

Figure 3. The reduced energies u_T and u_S of the strictly 2D triangular and square lattices, respectively, and their image systems. Energy is plotted against the parameter η which determines the relative image strength, $(-\eta)^l$, for the lth image plane relative to the real dipole array. Results are given for $\Delta = 0.8$, 1.0, 1.2 and ∞. This parameter, the ratio of fluid thickness to triangular lattice parameter, determines the reduced distance from a dipole to its first image. For this reason $u(\Delta = \infty)$ is independent of η. Note that for given Δ and η the triangular system always has the lower energy. The linearity of u with η shows that the first ($l = \pm 1$) image planes provide the dominant image contribution to u (see text).

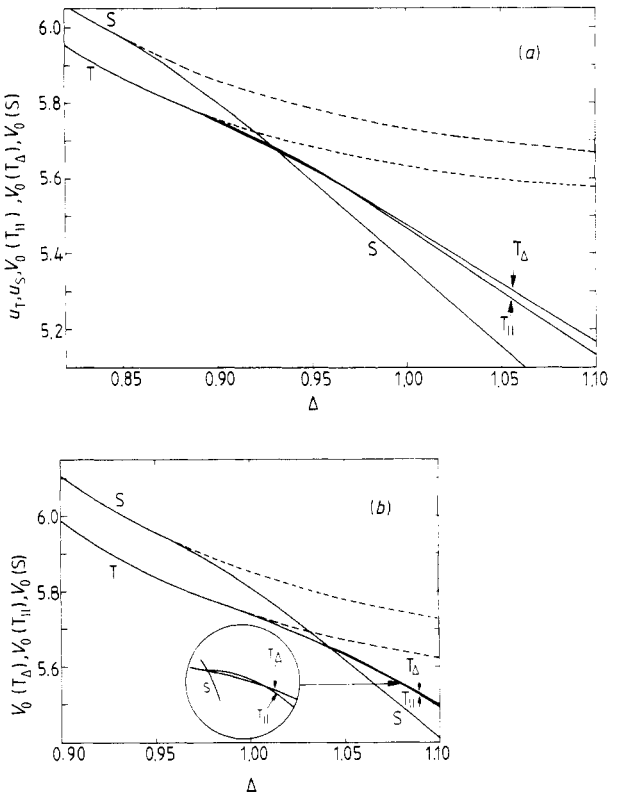

Figure 4. The reduced energies of undistorted and distorted triangular and square lattices as a function of Δ, the fluid thickness reduced by the lattice spacing of the triangular lattice. The parameter η governing the strength of images is (*a*) $\eta = 0.52$, corresponding to the experiments of Skjeltorp (1983) and (*b*) $\eta = 1.0$, the maximum possible value obtained when the ferro-fluid has a very high permittivity. The full line corresponds to the minimum energy for each lattice, the broken continuation being the energy only when distortions are suppressed. The distorted square becomes stable with respect to the distorted triangular system when (*a*) $\Delta > 0.93$, (*b*) $\Delta > 1.04$.

and the effective normalised thickness is $\Delta_S = (2/\sqrt{3})^{1/2}\Delta$ (see (22)). Note that the lattice energies scale essentially linearly with η. This reflects the fact that the contributions from successive image planes die away exponentially and thus only the first, with weight η, effectively contributes. It is therefore interesting to tabulate the results for each plane (l) for a particular case, that of a square lattice with $\Delta_S = 1$, where the ferro-fluid thickness equals the actual spacing of the square lattice (see table 1).

To get the total energy of a dipole interacting with other dipoles and all images one must take each plane, l (with the plane $-l$ if $|l| > 0$), and weight it by $(-\eta)^{|l|}$ in a sum over all planes. The rapid decay with increasing $|l|$ illustrates the exponential decay demanded by $\nabla^2\Phi = 0$ and explains the linearity in figure 3. Table 1 also provides an independent check on our procedure since, by setting $|\eta| = 1$, we obtain the limits discussed by Cohen and Keffer (1955).

(i) $\eta = 1$: planes stacked anti-ferromagnetically. This is their Z_2 limit. We find $2u_S = 9.687\,441$, in agreement with Cohen and Keffer.

Table 1. Interaction fields of individual image and real dipole planes for a square lattice with $\Delta_s = 1 \rightarrow \Delta = 0.9306$. These are twice the energies, as noted in § 2.

Plane l	Field per plane
0	9.033 619
1	$-3.274\,647 \times 10^{-1}$
2	$-5.549\,778 \times 10^{-4}$
3	$-1.028\,991 \times 10^{-6}$

(ii) $\eta = -1$ (unphysical in the context of magnetostatic images): ferromagnetic stacking. This is the longitudinal limit of $k \rightarrow 0$ for which the result is exactly $8\pi/3$ (Cohen and Keffer). This is again in accord with results in table 1 which give $2u_S = 8.377\,58$.

Since $u_S - u_T$ depends upon the value of η we show, in figure 4(a), u_T and u_S as functions of Δ for $\eta = 0.52$ (which corresponds to $\chi_f = 4\pi(0.17)$, the susceptibility of the magnetic colloid used by Skjeltorp (1983)) and in figure 4(b), u_T and u_S for $\eta = 1.0$, its largest possible value. We see from the figures that $u_T < u_S$, thus the triangular lattice is the more stable of the two configurations. Note that this result would *not be affected* by including dipole field corrections in u_T and u_S.

In summary, we find that the interaction energies of the underlying strictly 2D lattices and their image systems are extremely close (differing from each other by approximately 1%) with that of the triangular lattice being lower than that of the square one.

3.3. Results for the distorted lattices

The lattice sums required in order to calculate (to lowest order) the energies of the distorted square and triangular lattices relative to those of the undistorted structures, were given in § 2.3. Since these sums are proportional to either $1/r^5$ or $1/r^7$, they converge much more rapidly than those needed for the undistorted case. We could therefore evaluate them to the desired accuracy by direct numerical summation. The results for the three distortion modes considered by us are given graphically as a function of Δ for $\eta = 0.52$ and $\eta = 1.0$ in figures 4(a) and 4(b), respectively.

For $\eta = 0.52$ we find that the strictly planar square lattice structure becomes *unstable* with respect to the distortion mode of figure 2(a) when $\Delta > 0.85$. The triangular lattice, on the other hand, remains stable until $\Delta \simeq 0.88$, at which point it becomes unstable with respect to the triangular distortion mode (T_Δ) of figure 2(b). The energy of the distorted square lattice decreases more rapidly with increasing Δ than that of the triangular one and, for $\Delta > 0.93$, the square structure has the lower energy. Also, it is interesting to note that for higher values of Δ, $u_{T_\parallel} < u_{T_\Delta}$. That is, when *only* triangular lattice configurations are considered, the energetically preferred structure changes from undistorted to three-sublattice distortion pattern to two-sublattice distortion pattern with increasing Δ. However, this change in the triangular lattice pattern occurs in the regime in which the distorted square lattice is the true stable structure.

For $\eta = 1$ (see figure 4(b)), the results are qualitatively similar to that for $\eta = 0.52$. Here the square lattice is energetically preferred for $\Delta > 1.04$.

Finally, we note that the equilibrium values $\xi^2(\Delta, \eta)$ found from (17a) are indeed small, satisfying $\xi^2 < 0.04$ for $\Delta < 1.2$ and $\xi^2 < 0.06$ for $\Delta < 1.5$.

4. Discussion and conclusions

The main results of our analysis may be summarised as follows

(a) In a sufficiently strong external field applied perpendicular to the paramagnetic layer, a collection of spherical non-magnetic inclusions will crystallise in a 2D array.

(b) For sufficiently small layer thickness, the structure will be strictly 2D (i.e., the centres of all the spheres will be coplanar) and will form a triangular lattice.

(c) As the layer thickness is increased, the 2D triangular array becomes *unstable* with respect to displacements of the spheres perpendicular to the lattice plane. The structure is then quasi 2D and consists of three interlocking sublattices, located above, on, and below the initial plane (see figure 2(*b*)). The displacements are small for layer thicknesses of experimental interest.

(d) At still greater layer thicknesses, we find that the triangular array is no longer the state of minimum energy. Instead, a quasi 2D square array is predicted to be the energetically preferred configuration. Here the square array is arranged in two sublattices, such that the nearest neighbours of a given sphere are all on the other sublattice. The spheres on one sublattice lie above and those on the other below the layer medium.

Experimentally, Skjeltorp (1983, 1984) has studied the crystallisation of monodispersed polystyrene spheres in a paramagnetic fluid. This fluid (Type EHG 905, manufactured by Ferrofluidics Corporation) has an initial susceptibility of (in SI units) $\chi_f = 4\pi(0.17)$. Thus $\bar{\chi}_f = 0.88$ and $\eta = 0.52$. Skjeltorp studied two systems, both of which crystallised in triangular arrays. In the first, spheres of 1.9 μm diameter were used and the approximate lattice spacing was $a = 4.3$ μm. Thus

$$\gamma = V\bar{\chi}_f/8\pi a^3 = 1\times10^{-3}$$

and the dipole-field correction term is indeed negligible. The layer thickness in this system was fixed by using a low concentration of 5 μm spheres as spacers. However, there were indications (Skjeltorp, private communication) that these spheres were compressed and thus the actual thickness was probably less than the nominal one of 5 μm. Thus, for this system, $\Delta \leqslant 1.1$.

The second system used spheres of diameter 10 μm with a lattice spacing of approximately 15 μm. Thus, in this case,

$$\gamma = V\bar{\chi}_f/8\pi a^3 = 5\times10^{-3},$$

as noted in § 3. The nominal layer thickness was 15 μm and we have $\Delta \simeq 1$.

Theoretically, for $\eta = 0.52$, we have found that a triangular array should be stable only for layer thicknesses satisfying $\Delta < 0.93$. At larger values of Δ, a square lattice configuration is energetically preferred. Such a configuration has not been observed by Skjeltorp. This may possibly be due to the actual thickness of his experimental systems being somewhat less than their nominal values. Further experiments to clarify this point are clearly needed.

In addition to our prediction that a square lattice will exist for Δ sufficiently large, we also expect a *continuous* transition from a true 2D triangular structure to one that is only quasi 2D when Δ is increased from 0.85. Experimental verification of this prediction would also be of interest. One way of doing this would be to measure the effective dielectric constant of the system as a function of Δ. This will have a different functional dependence on Δ below and above the distortion threshold.

Finally, we note that Skjeltorp has suggested using these systems to study melting in two dimensions by varying the applied magnetic field and thereby varying the effective temperature. He has compared results found by this technique with those of molecular-dynamics computer simulations. However, as a consequence of the image dipoles which effectively exist in these systems, they are not truly two dimensional in character. Thus comparisons with 2D simulations must be regarded cautiously.

Another possibility for melting also suggests itself as a consequence of our investigations of energetically driven distortional instabilities. For a Δ such that a planar system was close to distorting out of plane perhaps melting to a distortionally disordered but still triangular phase will intervene before positional melting. The value of such a melting temperature, should it exist, will scale not only with the applied magnetic field but with Δ and η which govern distortions out of plane. As we mentioned before, this is a situation with certain similarities with the Blume-Emry-Griffiths model with spins of magnitude 1 on a triangular lattice. However the interaction, like $1/r^5$, gives us differences from that model. The worries about the 3D image assembly persist.

Acknowledgments

We thank Professor R J Elliott and the Department of Theoretical Physics, Oxford for their hospitality during the period when this work was carried out. MW thanks Dr J M F Gunn for frequent discussions.

Appendix. A modification of the Ewald method of summation

As explained by Nijboer and de Wette (1957) the Ewald method circumvents the poor convergence of dipole sums by partially summing in reciprocal or Fourier space where convergence is consequently good. We indicated in § 3 that modification is needed when the summation must proceed by grouping into planes. We therefore briefly review the method and introduce the necessary changes.

Let the summand be $f(\boldsymbol{r}_\lambda)$ where $\boldsymbol{\lambda}$ indicates a lattice point, in this case in real space, but also, for $\boldsymbol{k}_\lambda$, in Fourier space. In our problem

$$f(\boldsymbol{r}_\lambda) \propto Y_{20}(\theta_{\boldsymbol{r}_\lambda+\boldsymbol{R}})/|\boldsymbol{r}_\lambda - \boldsymbol{R}|^3, \tag{A1}$$

where Y_{20} is the second spherical harmonic and (A1) corresponds to (3*b*). The 2D lattice vector $\boldsymbol{r}_\lambda$ is in the dipole plane and $\boldsymbol{R}$ is a vector perpendicular to the plane to the point at which the resultant field is to be evaluated.

Because of its dipole origin, $f(\boldsymbol{r}_\lambda)$ is slowly convergent. Now, a sum over all lattice points can be rearranged identically in the form:

$$\sum_\lambda f(\boldsymbol{r}_\lambda) = \sum_\lambda f(\boldsymbol{r}_\lambda)\phi(\boldsymbol{r}_\lambda) + \sum_\lambda f(\boldsymbol{r}_\lambda)(1-\phi(\boldsymbol{r}_\lambda)), \tag{A2}$$

where $\phi(\boldsymbol{x})$ is an otherwise arbitrary function which decays rapidly to zero as $\boldsymbol{x} \to \infty$ and approaches unity as $\boldsymbol{x} \to 0$. The first part can now be evaluated conventionally; the second part has the same poor convergence at large $\boldsymbol{r}_\lambda$ as before but, in addition, is flat at small $\boldsymbol{r}_\lambda$. A flat function in real space is sharply peaked in $\boldsymbol{k}$ space, as exemplified in an extreme form by the δ function. The transformation to $\boldsymbol{k}$ space is

effected by first setting

$$\sum_{\lambda} f(1-\phi) \equiv \int \mathrm{d}\boldsymbol{r}\, \omega(\boldsymbol{r})(1-\phi(\boldsymbol{r}))f(\boldsymbol{r}) \tag{A3}$$

with

$$\omega(\boldsymbol{r}) = \sum_{\lambda} \delta(\boldsymbol{r}-\boldsymbol{r}_{\lambda}). \tag{A4}$$

The right-hand side of (A3) is further transformed using Parcevals theorem

$$\int \omega(\boldsymbol{r})(1-\phi(\boldsymbol{r}))f(\boldsymbol{r})\,\mathrm{d}\boldsymbol{r} \rightarrow \int \mathrm{d}\boldsymbol{k}\, \hat{\omega}(\boldsymbol{k})\mathrm{FT}[(1-\phi)f] \tag{A5}$$

where $\hat{\omega}(\boldsymbol{k})$ is the Fourier transform (FT) of $\omega(\boldsymbol{r})$:

$$\begin{aligned}\hat{\omega}(\boldsymbol{k}) &= \int \mathrm{d}\boldsymbol{r} \exp(2\pi \mathrm{i}\boldsymbol{k}\cdot\boldsymbol{r})\omega(\boldsymbol{r}) \\ &= \sum_{\lambda} \exp(2\pi \mathrm{i}\boldsymbol{k}\cdot\boldsymbol{r}_{\lambda}) \equiv \frac{1}{v}\sum_{\lambda}\delta(\boldsymbol{k}-\boldsymbol{k}_{\lambda})\end{aligned} \tag{A6}$$

where v is the volume (area) of a unit cell of the real lattice. Sums (in $\boldsymbol{k}$ space) are now obtained by substituting (A4) into (A5) to give

$$\frac{1}{v}\sum_{\lambda}\mathrm{FT}\{(1-\phi)f\}_{\boldsymbol{k}=\boldsymbol{k}_{\lambda}}. \tag{A7}$$

A good choice for the separation function ϕ has been shown by Nijboer and de Wette (1957) to be the incomplete gamma function, $\Gamma(n, x)$. Convergence in real space is extremely rapid and the Fourier transforms $(1-\Gamma)f$ for functions f commonly encountered (inverse powers and Legendre polynomials) are easily obtained and yield rapidly convergent k-space sums.

To this point we have not specified the spatial dimension of the lattices and hence the sums and integrals involved. Nijboer and de Wette (1957) have shown how to treat sums where (a) the origin is either a lattice point ($\boldsymbol{R}=0$) or (b) the origin is displaced a distance $\boldsymbol{R}$ from a lattice point, where $\boldsymbol{R}$ is a vector in the space of the lattice, e.g. in 2D when the lattice vectors $\boldsymbol{r}_{\lambda}$ span a 2D lattice. In our case $f(\boldsymbol{r}_{\lambda})$ involves an $\boldsymbol{R}$ orthogonal to the lattice vectors $\boldsymbol{r}_{\lambda}$. We therefore proceed by first carefully specifying, in (A3) to (A7), the dimensionalities of the relevant quantities by appropriate subscripts and superscripts:

$$\sum_{\lambda} f(1-\phi) \equiv \int \mathrm{d}^3\boldsymbol{r}\, \omega(\boldsymbol{r})(1-\phi(\boldsymbol{r}))f(\boldsymbol{r}) \tag{A3b}$$

$$\omega(\boldsymbol{r}) = \sum_{\lambda}^{2\mathrm{D}} \delta_3(\boldsymbol{r}-\boldsymbol{r}_{\lambda}), \tag{A4b}$$

$$\int \omega(1-\phi)f \rightarrow \int \mathrm{d}^3\boldsymbol{k}\, \hat{\omega}(\boldsymbol{k})\mathrm{FT}_3\{(1-\phi)f\} \tag{A5b}$$

$$\hat{\omega}(\boldsymbol{k}) = \frac{1}{v}\sum_{\lambda}^{2\mathrm{D}} \delta_2(\boldsymbol{k}_{\perp}-\boldsymbol{k}_{\lambda}). \tag{A6b}$$

Now v is the unit cell area of the 2D real lattice and $\boldsymbol{k}_\perp$ is the component of $\boldsymbol{k}$ in the plane of the reciprocal space spanned by the 2D $\boldsymbol{k}_\lambda$.

Nijboer and de Wette show that an appropriate splitting function $\phi(r)$ is

$$\phi(\boldsymbol{r}) = \Gamma(5/2, \pi r^2)/\Gamma(5/2)$$

and that $(1-\phi(\boldsymbol{r})) = \gamma(5/2, \pi r^2)/\Gamma(5/2)$ (here $\gamma(n, x) = \Gamma(n) - \Gamma(n, x)$ is the complementary form) has the Fourier transform

$$\frac{1}{v}\mathrm{FT}_3\left(\frac{\gamma(5/2, \pi r^2)}{r^3} Y_{20}(\theta_r)\right) = \frac{\mathrm{i}^2\pi^{3/2}}{v}\Gamma(1, \pi k^2) Y_{20}(\theta_k). \tag{A7b}$$

Given that our f in (A1) is displaced by the vector $\boldsymbol{R}$ we must, according to the usual rules of Fourier transforms, multiply (A7b) by $\exp(2\pi \mathrm{i}\boldsymbol{k}\cdot\boldsymbol{R}) \equiv \exp(2\pi \mathrm{i}k_\parallel R)$ where $k_\parallel$ is the component of $\boldsymbol{k}$ orthogonal to the $\boldsymbol{k}_\lambda$ plane. Inserting (A6b) for $\hat{\omega}(\boldsymbol{k})$ and (A7b) for $\mathrm{FT}\{(1-\phi)f\}$ into (A5b), and noting that $\int \mathrm{d}\boldsymbol{k}\,\delta_2 \to \int \mathrm{d}k_\parallel\,\mathrm{d}^2\boldsymbol{k}_\perp \delta(\boldsymbol{k}_\perp - \boldsymbol{k}_\lambda)$ can be reduced as a consequence of the δ-function acting in two of the three dimensions, the $\boldsymbol{k}$-space part of the summand becomes

$$\frac{-\pi^{3/2}}{v\Gamma(5/2)} \sum_{\lambda}^{2\mathrm{D}} \int \mathrm{d}k_\parallel\, \Gamma(1, \pi(k_\lambda^2 + k_\parallel^2)) Y_{20}(\theta_{k_\lambda + k_\parallel}) \exp(2\pi \mathrm{i}k_\parallel R). \tag{A8}$$

We can further reduce this expression since $\Gamma(1, x)$ is elementary (a simple exponential) and $Y_{20}(\theta) \propto (1 - \frac{3}{2}\sin^2\theta)$ whence the integral in (A8) becomes

$$\int \mathrm{d}k_\parallel \exp(2\pi \mathrm{i}k_\parallel R - \pi k_\parallel^2) \cdot [1 - \tfrac{3}{2}k_\lambda^2/(k_\lambda^2 + k_\parallel^2)]. \tag{A9}$$

The first part of (A9) is, by completion of the square, simply $\exp(-\pi R^2)$. The second part is reducible to the complementary error function multiplied by Gaussians. To see this, use the parametrisation

$$\frac{1}{k_\lambda^2 + k_\parallel^2} = \frac{1}{2k_\lambda} \int \mathrm{d}\chi \exp(\mathrm{i}\chi k_\parallel - k_\lambda|\chi|) \tag{A10}$$

do the $\int \mathrm{d}k_\parallel$ and finally, via a change of variable, $\int \mathrm{d}\chi$. The result is the sum of the two terms (with + and −)

$$-\tfrac{3}{4}\pi k_\lambda \exp[-\pi R^2 + \pi(k_\lambda \pm R)^2] \operatorname{erfc}(\pi^{1/2}(k_\lambda \pm R)). \tag{A11}$$

Having evaluated the k-space part of the sum, we combine it with the first (real space) part in (A2) to obtain the overall result (21) given in § 3.

The incomplete gamma function is related to elementary functions via the recursion relation

$$\Gamma(a+1, x) = a\Gamma(a, x) + x^a \mathrm{e}^{-x} \tag{A12}$$

and, since a is half-integral, we can also use

$$\Gamma(-\tfrac{1}{2}, x^2) = \pi^{1/2} \operatorname{erfc}(x) = 2\int_x^\infty \mathrm{e}^{-t^2}\,\mathrm{d}t, \tag{A13}$$

whence (21) reduces to Gaussians, complementary error functions and exponentials in addition to the $1/r^3$ factor. Thus all the sums in (21) are seen to be extremely rapidly convergent.

When R is large, the largest terms in (21) come from those k_λ taking their smallest non-zero values and considering the contribution with the $(-)$ sign in the last term involving erfc. This leading term is indeed exponentially decaying in R as required by the general argument given in § 3.

When $\boldsymbol{R}=0$ we have the sum over the plane of real dipoles. The angular factor Y becomes a constant and we naturally exclude from the sum the contribution at the origin ($r_\lambda=0$) the resultant field is being evaluated. The case $\boldsymbol{R}=0$ is a standard problem (see Nijboer and de Wette 1957). Excluding the origin, one obtains for the in-plane sum

$$\frac{1}{\Gamma(5/2)}\left(\sum_\lambda{}' \Gamma(\tfrac{3}{2}, \pi r_\lambda^2)/r^3+\frac{\pi^2}{v}k_\lambda\Gamma(-\tfrac{1}{2}, \pi k_\lambda^2)+\left(\frac{2}{v}-\frac{2}{3}\right)\pi^{3/2}\right) \tag{A14}$$

where the prime on Σ indicates this exclusion. One can then reduce (21) to (A14) by letting $R\to 0$, using (A12) to reduce the order of Γ, (A13) to introduce erfc and noting that

$$\sum_\lambda{}' \exp(-\pi r_\lambda^2)\equiv\frac{1}{v}-1+\frac{1}{v}\sum_\lambda{}' \exp(-\pi k_\lambda^2). \tag{A15}$$

References

Bleaney B I and Bleaney B 1978 *Electricity and Magnetism* (Oxford: OUP) chap 4

Blume M, Emry V and Griffiths R 1971 *Phys. Rev.* A **4** 1071

Cohen M H and Keffer F 1955 *Phys. Rev.* **99** 1128

Nijboer B R A and de Wette F W 1957 *Physica* **23** 309

Rosensweig R E 1966 *Nature* **210** 613

—— 1979 *Advances in Electronics and Electron Physics* vol 48, ed L Marton (London: Academic) pp 103–201

Skjeltorp A T 1983 *Phys. Rev. Lett.* **51** 2306

—— 1984 *J. Appl. Phys.* **55** 2587

Weber E 1950 *Electromagnetic Fields: Theory and Applications* vol 1 (New York: Wiley) p 218